Heliyon 5 (2019) e01976

Contents lists available at ScienceDirect

Heliyon

www.elsevier.com/locate/heliyon

Periodic low-frequency electric field structures in a magnetized non-thermal auroral plasma

O.R. Rufai *

University of the Western Cape, Robert Sobukwe Rd, Bellville 7535, Cape Town, South Africa

ARTICLE INFO

Keywords:
Computational mathematics
Geophysics
Nonlinear physics
Plasma physics
Wave physics
Auroral plasma
Low-frequency
Quasi-neutrality condition
Non-thermal electrons
Electric field structures

ABSTRACT

The theoretical explanation of electric field structures associated with density depletion in the Earth's upper ionosphere is presented. Using the quasi-neutrality hypothesis, the effect of excess energetic electron species is studied on the evolution of nonlinear low-frequency ion-cyclotron and ion-acoustic waves in a magnetized auroral plasma. The dynamics of the cold ion beam is governed by the fluid equations and the electron is treated as energetic species with non-thermal density distribution. Numerical computations appear in a series of periodic oscillations, such as spiky, sawtooth and sinusoidal waveforms. The present model can generate up to 18 mV/m electric field amplitude, which is in the range of the FREJA satellite measurements in the auroral acceleration region.

1. Introduction

Broadband electrostatic noise (BEN) have been observed with frequencies fluctuating from the ion-cyclotron up to and higher than the ion plasma frequency (frequency range of several hectohertz (hHz) to a few kilohertz (kHz)) in the auroral acceleration region of the Earth's magnetosphere [1]. Several spacecraft missions have reported that BEN has a potential of dynamical characters with small-scale, large-amplitude, magnetic-aligned electric fields in different regions of the magnetosphere, e.g. in the auroral acceleration region [2], the plasma sheet boundary layer (PSBL) [3], polar cup boundary layer (PCBL) [4], the Earth's high altitude polar magnetosphere [5], on cusp field lines [6] and magnetosheath [7], etc.

Further investigations revealed that BENs consist of non-linear, quasi-static, time-domain parallel or/and perpendicular electric field structures, such as spiky, sawtooth and sinusoidal structures in an electrostatic ion cyclotron (EIC) wave reported by S3-3 [8], Viking [9], FREJA [10], POLAR [11, 12] and FAST [13] satellites. Various theoretical investigations of such electric field structures parallel and perpendicular to the geomagnetic field line have been done by several authors [14, 15, 16, 17, 18] using the fluid theory technique. In order to explain the generating mechanism of the parallel electric field fluctuations which exhibit sawtooth or spiky wave structures observed by FAST satellite mission, Reddy et al. [14] presented a magnetized two-component auroral plasma model consisting of a cold ion and Boltzmann electron distribution, which is responsible for the field-aligned current. The investigation reveals series of non-linear structures, such as sinusoidal, sawtooth and spiky waveforms.

The instruments on the Viking [9] and FREJA [10] satellite have detected a localized electrostatic structures in the lower hybrid wave frequency of the Earth's upper atmosphere with characteristic features of a density depletion supported by an enhancement of the electric field fluctuations, which appear as wave-filled cavities with strong potential drop along the geomagnetic field line of the Earth's magnetosphere. Such observed non-linear electrostatic structures might be found to exist predominantly in regions where high-energy particles accelerated or during the magnetic reconnection. A pattern of such fluctuations is shown in Fig. 1, where the period of oscillation of the wave propagation along the magnetic field line is found to be small [19]. These observed structures are generally associated with beams of energized ions flowing in upward directions and electrons being decelerated along the geomagnetic field line and form the aurora when infiltrate into the auroral acceleration region of the Earth's upper atmosphere [9]. Motivated by the spacecraft measurements, several theoretical attention have been focused on the presence of the excess energetic particles as the generating mechanism of electrostatic structures with density

* Corresponding author.
E-mail address: orufai@uwc.ac.za.

https://doi.org/10.1016/j.heliyon.2019.e01976
Received 5 February 2019; Received in revised form 18 April 2019; Accepted 17 June 2019

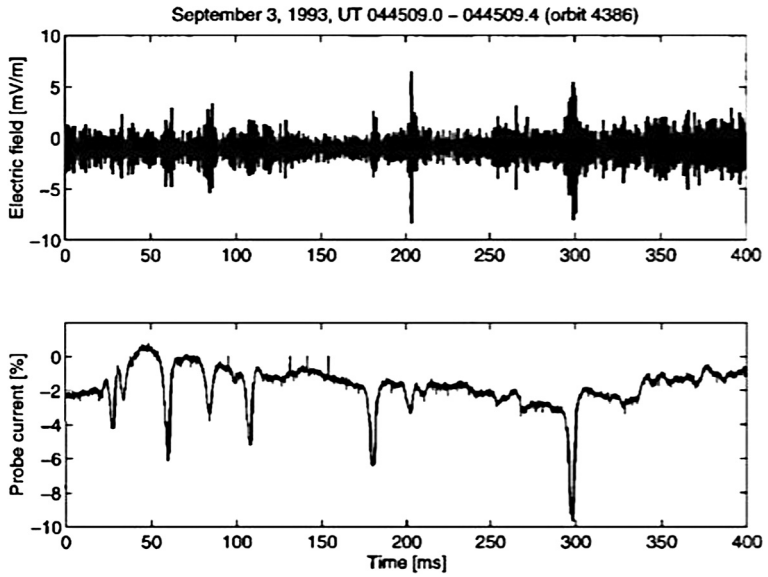

Fig. 1. The electric field structures observed by FREJA satellite (taken from Kjus et al. [19]).

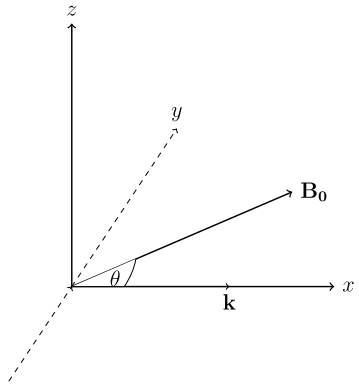

Fig. 2. Geometry of the model.

depletion in the Earth's magnetosphere. It has been found that the velocity distribution function of such particles completely deviated from Maxwellian-Boltzmann equilibrium. An example of such velocity distribution is Kappa [20], Tsallis q-nonextensive [21] and Cairn's non-thermal distribution [22].

In an attempt to describe the nonlinear structures observed in the Earth's upper ionosphere with density depletion, Cairns et al. [22] proposed a non-thermal velocity distribution function for the model of the excess energetic particles. In this paper, the Cairn's non-thermal velocity distribution will account for the density of the excess energetic electron species coupled with a cold ion beam drifting along the magnetic field with speed v_0 to investigate the properties of the electric field structures observed in the Earth's upper ionosphere, as an extension of Reddy et al. [14]. The format of this paper is as follows. Section 2 present the theoretical model and the numerical results in Section 3. Conclusions are drawn in Section 4.

2. Model

For the plasma model, a homogeneous, nonlinear low-frequency wave in a magnetized two-component collisionless plasma consisting of a cold ion beam and excess energetic electrons with non-thermal distribution is considered. The arbitrary amplitude ion-cyclotron (IC) and ion-acoustic (IA) waves are propagating obliquely in the x-direction at an angle θ to the magnetic field $\mathbf{B_0}$, which is assumed to be in the (x,z)-plane (see Fig. 2). On the ion time scale, the phase velocity of the oscillations is reckoned to be smaller in comparison with the electron thermal velocity, **which satisfies** $v_{Ti} \ll v_p/\gamma \ll v_{Te}$**, that is, the plasma wave is subject to Landau damping. Here** $v_j = \sqrt{\frac{T_j}{m_j}}$ **is the particle thermal velocity,** T_j **and** m_j **are particle temperature and mass, where** $j = i, e$ **for ions and electrons respectively**. Thus, the Cairn's [22] non-thermal velocity distribution function will be adopted for the excess energetic electron species. In unnormalized form, the Cairn's non-thermal electrons distribution function is given by

$$f_e(v) = \frac{n_0}{(3\alpha+1)\sqrt{2\pi v_e^2}}\left(1+\frac{\alpha v^4}{v_e^4}\right)\exp\left(-\frac{v^2}{2v_e^2}\right) \tag{1}$$

where n_0 is the equilibrium electron density and v_e is the thermal speed of the electrons and α is the non-thermal energetic electron parameter. Then, the non-thermal energetic electron distribution can be found by replacing v^2/v_e^2 by $v^2/v_e^2 - 2e\phi/T_e$ in Eq. (1), which, on integration over velocity space, gives the following expression for the electron density [22, 23, 26, 27]:

$$n_e = n_0\left[1-\beta\left(\frac{e\phi}{T_e}\right)+\beta\left(\frac{e\phi}{T_e}\right)^2\right]\exp\left(\frac{e\phi}{T_e}\right), \tag{2}$$

where the excess energetic electron component, $\beta = \frac{4\alpha}{1+3\alpha}$ and α measure the non-thermal electron population. For $0 \le \alpha \le \infty$, the value of β is limited in the range $0 \le \beta \le 4/3$. It is noted that $\alpha \to 0$ corresponds to the Boltzmann distribution limit of electrons.

The dynamics of the cold ion beam $(N_i, T_i = 0)$ are described by the fluid equations, namely the continuity and momentum equations [14],

$$\frac{\partial n_i}{\partial t} + \frac{\partial (n_i v_{ix})}{\partial x} = 0 \tag{3}$$

$$\frac{\partial v_{ix}}{\partial t} + v_{ix}\frac{\partial v_{ix}}{\partial x} = -\frac{e}{m_i}\frac{\partial \phi}{\partial x} + \Omega_i v_{iy}\sin\theta \tag{4}$$

$$\frac{\partial v_{iy}}{\partial t} + v_{ix}\frac{\partial v_{iy}}{\partial x} = \Omega_i v_{iz}\cos\theta - \Omega_i v_{ix}\sin\theta \tag{5}$$

$$\frac{\partial v_{iz}}{\partial t} + v_{ix}\frac{\partial v_{iz}}{\partial x} = -\Omega_i v_{iy}\cos\theta, \tag{6}$$

where n_i is the cold ion density, v_{ix}, v_{iy} and v_{iz} are the components of the ion velocity along the x, y and z directions, respectively, $\Omega_i (= e\mathbf{B}_0/m_i)$ is the ion cyclotron frequency, m_i is the ion mass, e is the magnitude of the electron charge and ϕ is the electrostatic potential of the waves. Then, the set of the equations are closed with the charge

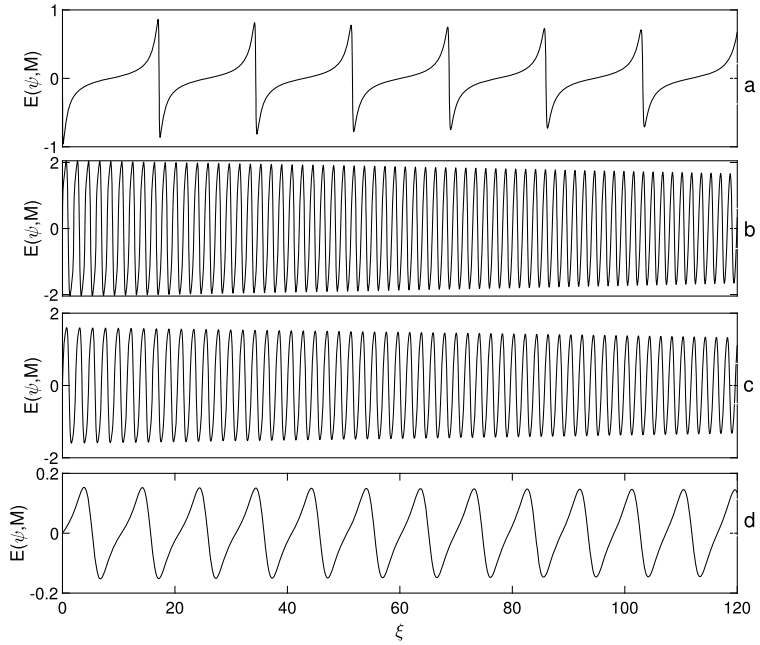

Fig. 3. Normalized electric field structures $E(\psi, M)$ vs ξ for $M = 1.25$, $\theta = 2°$, $\delta = 0.2$, $E_0 = 1.1$, $\alpha = 0.00$ (a), 0.05 (b), 0.1 (c), 0.199 (d).

neutrality condition ($n_i = n_e$), which is valid for low-frequency analysis [23, 24, 28, 29].

The non-linear analysis of Eqs. (3) to (6) that depend on space x and time t can be done through a stationary frame $\xi = (x - Vt)\Omega_i/V$, where V is the phase velocity of the wave. Using the quasi-neutrality condition and the following initial conditions, $n_i = n_0$ and $v_x = v_0$ at $\xi = 0$. In addition, the normalized electric field potential $\psi = e\phi/T_e$, Mach number $M = V/C_s$ and $\delta = v_0/C_s$, where $C_s = (T_e/m_i)^{1/2}$ is the ion-acoustic speed. Then, Eq. (3) becomes

$$v_x' = \frac{-(V - v_0)e^{-\psi}}{(1 - \beta\psi + \beta\psi^2)}, \tag{7}$$

by eliminating the ion-velocity components, v_x and v_z from Eqs. (4) to (6) and exploiting Eq. (7) to obtain

$$\frac{d}{d\xi}\left[\frac{e^{-\psi}}{1 - \beta\psi + \beta\psi^2}\left(\frac{d^2\psi}{d\xi^2} + \frac{M_A^2 e^{-2\psi}}{(1 - \beta\psi + \beta\psi^2)^3}\left(-(1 + \beta\psi + \beta\psi^2 - \beta)\frac{d^2\psi}{d\xi^2}\right.\right.\right.$$
$$+((1 + \beta\psi + \beta\psi^2 - \beta)(2 + 3(2\beta\psi - \beta)(1 - \beta\psi + \beta\psi^2)^2)$$
$$\left.\left.\left.-(\beta + 2\beta\psi))\left(\frac{d\psi}{d\xi}\right)^2\right)\right)\right]$$
$$= -M^2\frac{d}{d\xi}\left(\frac{e^{-\psi}}{1 - \beta\psi + \beta\psi^2}\right) - \frac{M^2\cos^2\theta}{M_A^2}e^{\psi}(1 - \beta\psi + \beta\psi^2)\frac{d\psi}{d\xi} \tag{8}$$

where $M_A = M - \delta$.

Integrating Eq. (8) with the conditions $\psi = 0$, $d\psi/d\xi = E_0$ and $d^2\psi/d\xi^2 = 0$ at $\xi = 0$, to obtain a non-linear second-order differential equation of the form

$$\chi_1(\psi)\frac{d^2\psi}{d\xi^2} - \chi_2(\psi)\left(\frac{d\psi}{d\xi}\right)^2 + \chi_3(\psi) = 0, \tag{9}$$

where

$$\chi_1(\psi) = \frac{e^{-2\psi}(1 + \beta\psi + \beta\psi^2 - \beta)}{(1 - \beta\psi + \beta\psi^2)^3} - \frac{1}{M_A}, \tag{10}$$

$$\chi_2(\psi) = \frac{e^{-2\psi}((1 + \beta\psi + \beta\psi^2 - \beta)(2 + 3(2\beta\psi - \beta)(1 - \beta\psi + \beta\psi^2)^2) - (\beta + 2\beta\psi))}{(1 - \beta\psi + \beta\psi^2)^3}, \tag{11}$$

$$\chi_3(\psi) = e^{\psi}\left(\frac{M^2}{M_A^2} + 2(1 + \beta)(1 - 2\beta)E_0^2\right) - \frac{M^2}{M_A^2}$$
$$- \frac{M^2\cos^2\theta(1 - \beta\psi + \beta\psi^2)e^{\psi}}{M_A^2}\left(e^{\psi}(1 + \beta\psi + \beta\psi^2 - \beta) - (1 + 3\beta)\right). \tag{12}$$

Equation (9) describes the evolution of the nonlinear structures (both ion-cyclotron and ion-acoustic waves) in the auroral plasma. For the case of Boltzmann electron limit $\alpha = \beta \to 0$, Eqs. (10) to (12) goes back to Eqs. (11) to (13) of Reddy et al. [14]. In addition, perpendicular propagating electrostatic ion cyclotron (EIC) waves investigated by Temerin et al. [25] can be obtained for $\theta = 90$, $v_0 = 0$, $\alpha = \beta = 0$ and $E_0 = 0$, as a special case.

3. Results and discussions

The numerical computation of the nonlinear evolution equation (9) for low-frequency parallel electric field structures will be examined using the MATLAB ODE solver for periodic wave solutions in the electric field **E**. The results for the effect of the different auroral parameters, such as the non-thermal energetic electron contribution, α, Mach number, M, ion drift velocity, δ, electric field driver strength, E_0 and propagation angle, θ, are discussed.

The variation of normalized parallel electric field, $E(\psi, M)$ for $M = 1.25$ and vary the energetic non-thermal hot electrons as showed in Figs. 3(a) to (d) for other fixed parameters, $\theta = 2°$, $\delta = 0.2$ and the driver strength, $E_0 = 1.1$. The electric field curve plotted in Fig. 3(a) shows highly spiky waveform of driven ion acoustic mode in the absence of the non-thermal electron contributions α. This is a reciprocate of Fig. 7(d) of Reddy et al. [14] for the same plasma parameters. It is noted upfront (Fig. 3(a)) that in the limit $\alpha = \beta \to 0$, the Boltzmann limit [14] is obtained. In the present of the non-thermality component α (Fig. 3(b)), the period of the oscillations decreases and later grows to exhibit a sawtooth type at $\alpha = 0.199$ in Fig. 3(d). For $\alpha > 0.199$, no electric field structures can be found. This is consistent with the exceeding range of $\alpha > 0.25$, i.e. $\beta > 0.57$ the non-thermal distribution starts to earn ring component and particles become more energetic and might become unstable [23]. It is important to mention that the fluctuations in the electric field are found to be reduced due to the contribution of α. Therefore, one may concede that the electric field fluctuations, found to be small by the FREJA satellite (Fig. 1), arise due to the occur-

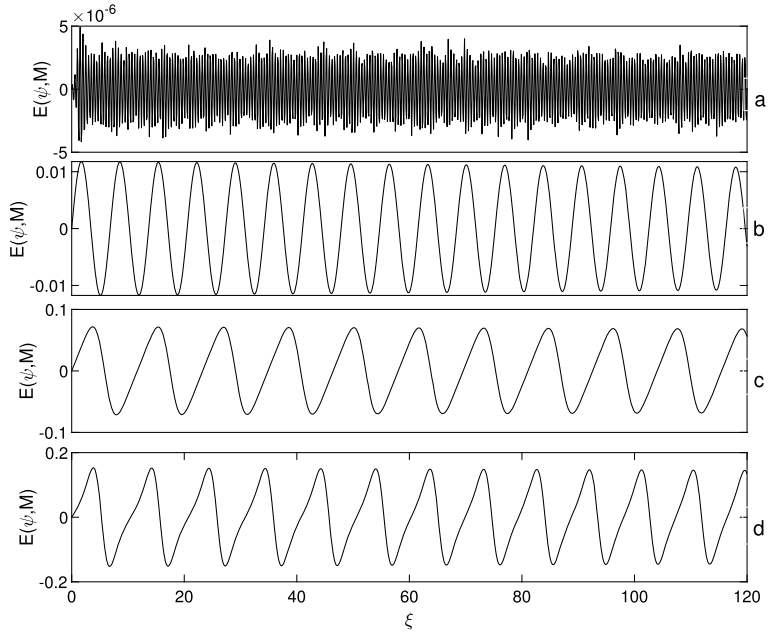

Fig. 4. Normalized electric field $E(\psi, M)$ vs ξ for $\alpha = 0.199$, $\theta = 2°$, $\delta = 0.2$, $E_0 = 1.1$, $M = 0.22$ (a), 1.0 (b), 1.20 (c), 1.25 (d).

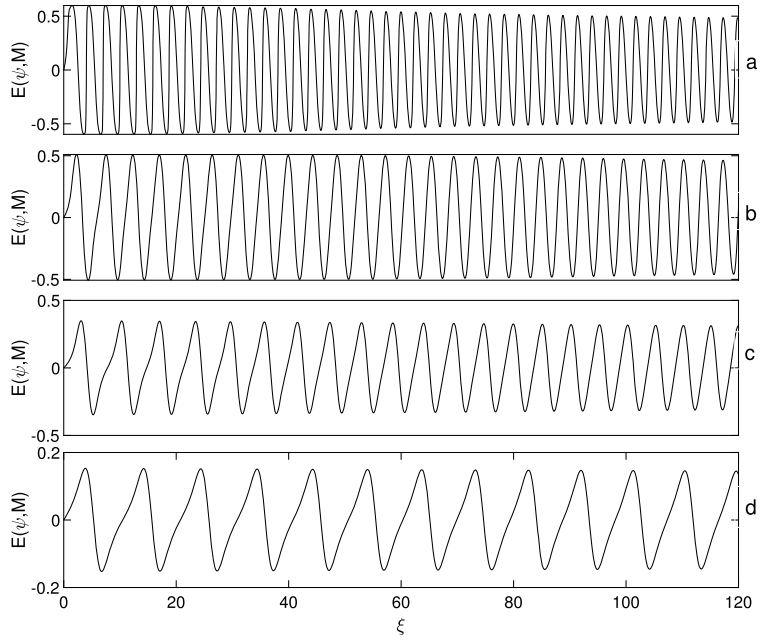

Fig. 5. Normalized electric field $E(\psi, M)$ vs ξ for $\alpha = 0.199$, $\theta = 2°$, $M = 1.25$, $E_0 = 1.1$, $\delta = -0.1$ (a), 0.0 (b), 0.1 (c), 0.2 (d).

rence of excess energetic particles attributed to the solar radiation in the Earth's magnetosphere. The period of the bipolar spiky structures with a period of approximately $\Delta t \cong \Delta\xi\ \Omega_i^{-1} \simeq 17\ \Omega_i^{-1} \approx 2.7\ \tau_{ci}$ (where the ion-cyclotron period is given by $\tau_{ci} = 2\pi/\Omega_i$) decreases to exhibit a sawtooth structure with a periodicity of about $\Delta\xi \simeq 7 \approx 1.1\tau_{ci}$ in Fig. 3(d). This structure is simply classified as an ion-acoustic mode.

The effect on normalized parallel electric field structures, $E(\psi, M)$ due to the variation in the Mach number is presented in Fig. 4(a)-(d) for a fixed non-thermal energetic hot electron of $\alpha = 0.199$ and other parameters of Fig. 3. For small values of Mach number, $M = 0.22$, the normalized parallel electric field exhibits a signal waveform, the fluctuations in the electric field are found to be small, that is, with low periodic oscillations. The wave frequency is very low to be captured similar to the FREJA spacecraft observations in Fig. 1. As the Mach number increases, the parallel electric field structures reveal the oscillations in the ion-cyclotron with sinusoidal behavior, which later tends to be of the sawtooth type with a period of about $\Delta t \approx 1.1\tau_{ci}$. It is obvious from the Fig. 4 that the period of the oscillations increases as the Mach number M increases from 0.22 to 1.25. This is due to the non-thermal electron effect, contrary to the case of Boltzmann electron [14]. It is also important to mention that no electric field structures can be found for $M < 0.22$, unlike the case of Boltzmann electron distribution studied by Reddy et al. [14], where the electric field structures can be found to exist for $M = 0.2$. In this case, a transition from ion-acoustic spiky to ion-cyclotron sinusoidal and back to ion-acoustic sawtooth structures are observed.

Fig. 5 illustrates the effect of the ion drift speed, δ on the normalized parallel electric field, $E(\psi, M)$ for $M = 1.25$ and other parameters

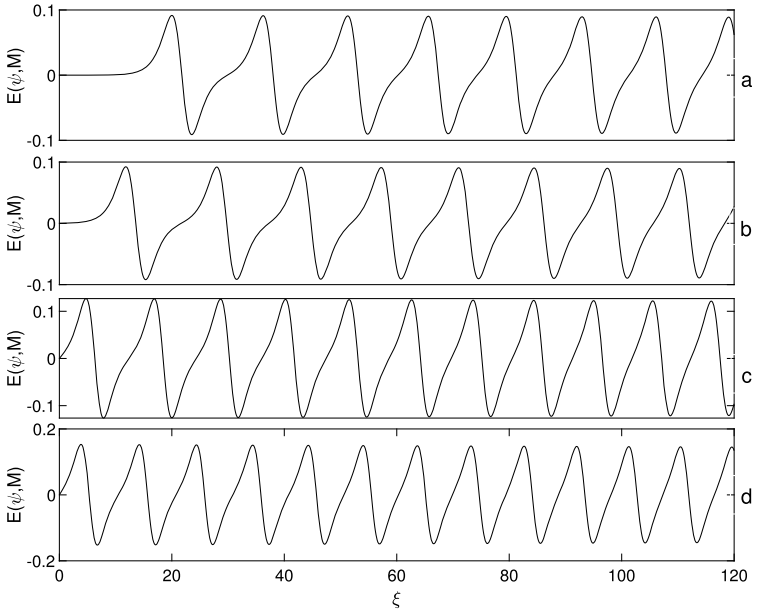

Fig. 6. Normalized electric field $E(\psi, M)$ vs ξ for $\alpha = 0.199$, $\theta = 2°$, $\delta = 0.2$, $M = 1.25$, $E_0 = 0.01$ (a), 0.1 (b), 0.8 (c), 1.1 (d).

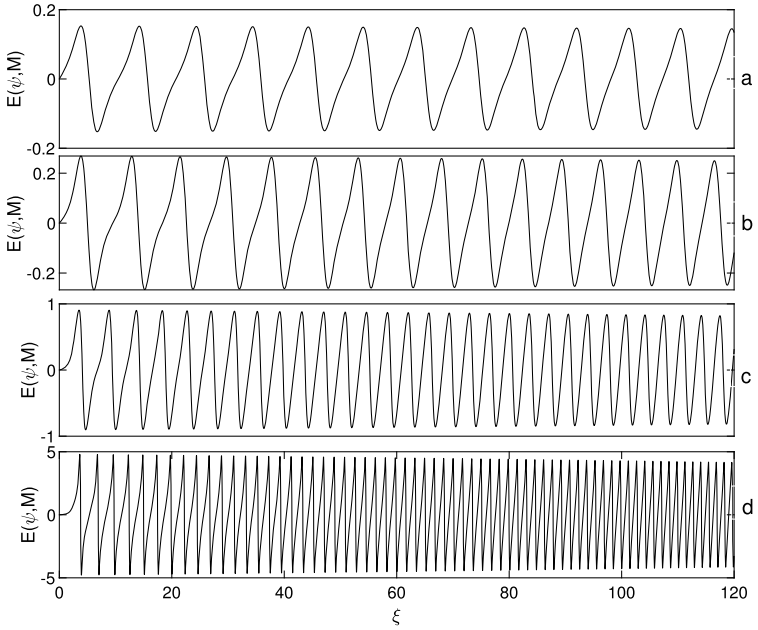

Fig. 7. Normalized electric field $E(\psi, M)$ vs ξ for $\alpha = 0.199$, $M = 1.25$, $\delta = 0.2$, $E_0 = 1.1$, $\theta = 2°$ (a), 20° (b), 50° (c), 85° (d).

of Fig. 4. The graphs showed the non-linear wave transformation from ion-cyclotron sinusoidal to ion-acoustic sawtooth structures. It is noted that the ion-cyclotron can be found propagating antiparallel to the magnetic field $\mathbf{B_0}$ (negative $-\delta$) which results to a sinusoidal electric field structure and later grown to ion-acoustic sawtooth type in the parallel magnetic field direction. The period of oscillation increases with the drift speed. The driven ion-cyclotron structure display in Fig. 5(a) has a low period of oscillation. For positive values of δ, the period of the oscillations grows faster as the direction of the ion flow becomes parallel to the magnetic field $\mathbf{B_0}$. The oscillation moves from a sinusoidal for $\delta = 0.0$ to a sawtooth type with a period of $\approx 1.1\tau_{ci}$ for $\delta = 0.2$. The present parallel electric field profile is contrary to the study of Reddy et al. [14], in which the period of the spiky structures decreases with δ.

In Fig. 6, the effect of the driver strength E_0 on the normalized parallel electric field profile is presented for $\alpha = 0.199$ and other fixed parameters of Fig. 4. The curves reveal only ion-acoustic sawtooth mode. For small driving amplitude $E_0 = 0.01$, the electric field oscillation period was found to be about $3.5\tau_{ci}$. As the driver strength E_0 increases, the ion-acoustic oscillation with sawtooth waveform decreases. On the same ion-acoustic sawtooth mode, the oscillation period reduce to about $1.1\tau_{ci}$ for large driven amplitude $E_0 = 1.1$. That is, the electric field potential amplitude drops with E_0, which may be related to the consequence of several different acceleration mechanisms responsible for the large scale potential drop along the geomagnetic field as observed by several spacecraft mission [9, 10].

Finally, the variation of the normalized electric field for the energetic non-thermal electrons $\alpha = 0.199$ and other fixed parameters of Fig. 4, for different values of the angle of propagation θ. As the angle of propagation θ increases from 2° (almost parallel propagation; Fig. 7(a)) to 85° (nearly perpendicular propagation; Fig. 7(d)) the period of the

oscillations decreases and a transition from the sawtooth to spiky structures occur with the mode remaining in the ion-acoustic regime. The curve in Fig. 7(d) shows the normalized electric field structures with lower period of oscillations for nearly perpendicular propagation. For the data captured from the FREJA satellite shown in Fig. 1, the electric field fluctuations in the magnetic field are found to be small. Therefore, one may infer that the low frequency waves may also propagate perpendicular to the magnetic field in the auroral region.

4. Conclusion

In this paper, the theoretical explanation of the periodic low-frequency non-linear electric field structures associated with density fluctuations in the auroral acceleration region of the Earth's magnetosphere have been presented. The auroral plasma model is composed of a cold ion beam and Cairn's non-thermal velocity distribution for excess energetic electron species. The study investigated the properties of non-linear low-frequency electrostatic fluctuations arising from a coupling of the ion-cyclotron and ion-acoustic waves in any direction of wave propagation to the ambient magnetic field in the presence of excess energetic electrons.

Regarding the spacecraft observation, the present study is merely looking for possible electric field structures in a non-thermal auroral plasma. The numerical computation presented here shows a sequence of wave bursts with the frequency of a small electric field fluctuations due to the contribution of the excess energetic electrons, which has a great resemblance with the observed structures by the FREJA spacecraft [10, 19]. It shows from the analysis that the FREJA observations (Fig. 1) can also be characterized either as nearly parallel or nearly perpendicular propagation wave modes as Reddy et al. [14] described the observation of FAST satellite in the auroral region. The plasma parameters, such as non-thermal contribution α, Mach number M, drift speed δ, electric field strength, E_0 and angle of propagation play roles in the existence of the non-linear structures. Furthermore, the energetic particles, such as electron/ion beams or the field-aligned currents are the source of the free energy responsible for generating electrostatic fluctuations in the auroral acceleration region. The model can generate wave structures with spiky, sawtooth and sinusoidal oscillations, and depending on the auroral plasma parameters both ion-cyclotron and ion-acoustic modes can be obtained. It has also shown the possibility of obtaining highly spiky electric field structures observed by FAST auroral satellite [13] as the limit of the non-thermal electron tends to zero ($\alpha = \beta \to 0$).

For the present model, the unnormalized electric field is given as [14, 17, 18]

$$E_{UN} = \frac{E}{M}\frac{T_e}{e\rho_i}. \tag{13}$$

Note that the ratio of the Mach numbers, $\frac{M_2}{M_1}$ is equal to the amplitudes of the electric field $\frac{E_1}{E_2}$, i.e., $E_1(E_2)$ is the electric field corresponding to the Mach number $M_1(M_2)$. In this paper, the electric field structures obtained are for electron temperature $T_e = 1 - 10$ eV [9] and the ion-cyclotron frequency of about $\Omega_i \approx 1000$ rad/sec. This would generate maximum ion acoustic speed, $C_s \approx 31$ km/s and electric field amplitude of about 18 mV/m from Eq. (13). These results may be relevant to the FREJA observations in Fig. 1 with electric field amplitude of the order of 20 mV/m or less by Kjus et al. [19].

The present theoretical analysis can be helpful in understanding the non-linear electrostatic fluctuations phenomena in space and astrophysics environments.

4.1. Derivation of the non-linear second-order differential equation

Defining the moving coordinate $\xi = (x - Vt)\Omega_i/V$, i.e. $\partial_x = \frac{\Omega_i}{V}\partial_\xi$, $\partial_t = -\Omega_i\partial_\xi$, the normalized fluid Eqs. (3)-(6) can be resolved. From Eq. (3)

$$V\frac{dn_i}{d\xi} - \frac{dn_i v_{ix}}{d\xi} = 0 \tag{14}$$

integrate

$$Vn_i - n_i v_{ix} = C \tag{15}$$

using the boundary conditions $\xi \to 0$, $v_{ix} = v_0$ and $n_i = n_0$, to obtain

$$v_x' n_i = -n_0(V - v_0) \tag{16}$$

where $v_x' = v_{ix} - V$ and $n_i = n_e$. Then, substituting equation (2) into equation (16) to obtain Eq. (7).

Then, one can write the Eqs. (4)-(6) in form

$$v_x'\frac{dv_{ix}}{d\xi} + \frac{e}{m_i}\frac{d\phi}{d\xi} = Vv_{iy}\sin\theta \tag{17}$$

$$v_x'\frac{dv_{iy}}{d\xi} = Vv_{iz}\cos\theta - Vv_{ix}\sin\theta \tag{18}$$

$$v_x'\frac{dv_{iz}}{d\xi} = -Vv_{iy}\cos\theta \tag{19}$$

Substituting Eq. (17) into Eq. (18) to obtain

$$v_{iz} = \frac{v_x'}{V^2\cos\theta\sin\theta}\left[\frac{d}{d\xi}\left(\frac{1}{2}\frac{dv_x'^2}{d\xi} + \frac{e}{m_i}\frac{d\phi}{d\xi}\right)\right] + \frac{v_{ix}\sin\theta}{\cos\theta}, \tag{20}$$

also, Eq. (17) into Eq. (19) gives

$$v_x'\sin\theta\frac{dv_{iz}}{d\xi} + v_x'\cos\theta\frac{dv_{ix}}{d\xi} + \cos\theta\left(\frac{e}{m_i}\frac{d\phi}{d\xi}\right) = 0. \tag{21}$$

Solving Eqs. (20) and (21) together to obtain

$$\frac{d}{d\xi}\left[v_x'\left(\frac{d}{d\xi}\left(\frac{1}{2}\frac{dv_x'^2}{d\xi} + C_s^2\frac{d\psi}{d\xi}\right)\right)\right] + V^2\frac{dv_{ix}}{d\xi} + \frac{V^2\cos^2\theta}{v_x'}C_s^2\frac{d\psi}{d\xi} = 0 \tag{22}$$

where $\frac{e\phi}{T_e} = \psi$ and $C_s^2 = \frac{T_e}{m_i}$.

Now, differentiating $v_{ix} = v_x' + V$ and use $v_x' = \frac{-(V-v_0)e^{-\psi}}{(1-\beta\psi+\beta\psi^2)}$ in Eq. (7) to obtain

$$\frac{dv_{ix}}{d\xi} = \frac{-(V-v_0)e^{-\psi}(\beta - \beta\psi - \beta\psi^2 - 1)}{(1-\beta\psi+\beta\psi^2)^2}\frac{d\psi}{d\xi}. \tag{23}$$

Substituting Eq. (23) into Eq. (22) and divide by $-(V - v_0)C_s^2$ gives

$$\frac{d}{d\xi}\left[\frac{e^{-\psi}}{1-\beta\psi+\beta\psi^2}\left(\frac{d^2\psi}{d\xi^2} + \frac{(M-\delta)^2}{2}\frac{d^2}{d\xi^2}\left(\frac{e^{-2\psi}}{(1-\beta\psi+\beta\psi^2)^2}\right)\right)\right] + M^2\frac{d}{d\xi}\left(\frac{e^{-\psi}}{1-\beta\psi+\beta\psi^2}\right) + \frac{M^2\cos^2\theta}{M_A^2}e^{\psi}(1-\beta\psi+\beta\psi^2)\frac{d\psi}{d\xi} = 0 \tag{24}$$

where $M = \frac{V}{C_s}$, $\delta = \frac{v_0}{C_s}$ and $M_A = M - \delta$. Integrate the Eq. (24) above to obtain

$$\frac{e^{-\psi}}{1-\beta\psi+\beta\psi^2}\left(\frac{d^2\psi}{d\xi^2} - \frac{M_A^2e^{-2\psi}(1-\beta\psi+\beta\psi^2-\beta)}{(1-\beta\psi+\beta\psi^2)^3}\frac{d^2\psi}{d\xi^2} + \left(\frac{(1+\beta\psi+\beta\psi^2-\beta)(2+3(2\beta\psi-\beta)(1-\beta\psi+\beta\psi^2)^2)-(\beta+2\beta\psi)}{(1-\beta\psi+\beta\psi^2)^3}\right) \times\left(\frac{d\psi}{d\xi}\right)^2\right) + \frac{M^2e^{-\psi}}{1-\beta\psi+\beta\psi^2} + \frac{M^2\cos^2\theta}{M_A^2}e^{\psi}(\beta\psi^2 - 3\beta\psi + 3\beta + 1) + C = 0 \tag{25}$$

then divide by $\frac{(1-\beta\psi+\beta\psi^2)}{M_A^2e^{-\psi}}$, using the boundary conditions $\psi = 0$, $d\psi/d\xi = E_0$ and $d^2\psi/d\xi^2 = 0$ at $\xi = 0$. The constant of integration C can be obtained as

$$C = -2(1+\beta)(1-2\beta)M_A^2E_0^2 - M^2 - \frac{M^2\cos^2\theta(1+3\beta)}{M_A^2}. \tag{26}$$

Finally, substitute Eq. (26) into Eq. (25) that gives

$$\left(\frac{e^{-2\psi}(1+\beta\psi+\beta\psi^2-\beta)}{(1-\beta\psi+\beta\psi^2)^3}-\frac{1}{M_A}\right)\frac{d^2\psi}{d\xi^2}$$
$$-\left(\frac{e^{-2\psi}((1+\beta\psi+\beta\psi^2-\beta)(2+3(2\beta\psi-\beta)(1-\beta\psi+\beta\psi^2)^2)-(\beta+2\beta\psi))}{(1-\beta\psi+\beta\psi^2)^3}\right)$$
$$\times\left(\frac{d\psi}{d\xi}\right)^2+e^{\psi}\left(\frac{M^2}{M_A^2}+2(1+\beta)(1-2\beta)E_0^2\right)-\frac{M^2}{M_A^2}$$
$$-\frac{M^2\cos^2\theta(1-\beta\psi+\beta\psi^2)e^{\psi}}{M_A^2}\left(e^{\psi}(1+\beta\psi+\beta\psi^2-\beta)-(1+3\beta)\right)=0. \quad (27)$$

Declarations

Author contribution statement

Odutayo R. Rufai: Conceived and designed the experiments; Performed the experiments; Analyzed and interpreted the data; Contributed reagents, materials, analysis tools or data; Wrote the paper.

Funding statement

This research did not receive any specific grant from funding agencies in the public, commercial, or not-for-profit sectors.

Competing interest statement

The authors declare no conflict of interest.

Additional information

No additional information is available for this paper.

References

[1] S.V. Singh, R.V. Reddy, G.S. Lakhina, Adv. Space Res. 28 (11) (2001) 1643–1648.
[2] M. Temerin, K. Cerny, W. Lotko, F.S. Mozer, Phys. Rev. Lett. 48 (1982) 1175.
[3] H. Matsumoto, H. Kojima, T. Miyatake, Y. Omura, M. Okada, M. Tsurutani, Geophys. Res. Lett. 21 (1994) 2915.
[4] B.T. Tsurutani, J.K. Arballo, G.S. Lakhina, C.M. Ho, B. Buti, et al., Geophys. Res. Lett. 25 (1998) 4117.
[5] J.R. Franz, P.M. Kintner, J.S. Pickett, Geophys. Res. Lett. 25 (1998) 1277.
[6] C.A. Cattel, J. Dombeck, J.R. Wygant, M.K. Hudson, F.S. Mozer, M.A. Temerin, W.K. Peterson, C.A. Kletzing, C.T. Russell, R.F. Pfaff, Geophys. Res. Lett. 26 (1999) 425.
[7] J.S. Pickett, J.D. Menietti, D.A. Gurnett, B.T. Tsurutani, P. Kintner, E. Klatt, A. Balogh, Nonlinear Process. Geophys. 10 (2003) 3.
[8] F.S. Mozer, M. Temerin, in: B. Hultqvist, L. Stenflo (Eds.), High-Latitude Space Plasma Physics, Plenum, New York, 1983, p. 453.
[9] R. Bostrom, B. Holback, G. Holmgren, Phys. Scr. 39 (1989) 782–786.
[10] P.O. Dovner, A.I. Eriksson, R. Bostrom, B. Holback, Geophys. Res. Lett. 21 (17) (1994) 1827–1830.
[11] F.S. Mozer, R. Ergun, M. Temerin, C. Cattell, J. Dombeck, J. Wygant, Phys. Rev. Lett. 79 (1997) 1281–1284.
[12] F.S. Mozer, C.A. Kletzing, Geophys. Res. Lett. 25 (11) (1998) 1629–1632.
[13] R.E. Ergun, C.W. Carlson, J.P. McFadden, F.S. Mozer, G.T. Delory, W. Peria, C.C. Chaston, M. Temerin, R. Elphic, R. Strangeway, R. Pfaff, C.A. Cattell, D. Klumpar, E. Shelley, W. Peterson, E. Moebius, L. Kistler, Geophys. Res. Lett. 25 (1998) 2025–2028.
[14] R.V. Reddy, G.S. Lakhina, N. Singh, R. Bharuthram, Nonlinear Process. Geophys. 9 (2002) 25–29.
[15] R.V. Reddy, S.V. Singh, G.S. Lakhina, R. Bharuthram, Earth Planets Space 58 (2006) 1227–1232.
[16] R. Bharuthram, R.V. Reddy, G.S. Lakhina, N. Singh, Phys. Scr. T 98 (2002) 137–140.
[17] S. Moolla, R. Bharuthram, S.V. Singh, G.S. Lakhina, R.V. Reddy, Phys. Plasmas 17 (2010) 022903.
[18] S. Moolla, I.J. Lazarus, R. Bharuthram, J. Plasma Phys. 78 (5) (2012) 545–551.
[19] S.H. Kjus, H.L. Pecseli, B. Lybekk, J. Holtet, J. Trulsen, H. Luhr, A. Eriksson, J. Geophys. Res. 103 (A11) (1998) 26,633–26,647.
[20] V.M. Vasyliunas, J. Geophys. Res. 73 (1968) 2839.
[21] C. Tsallis, J. Stat. Phys. 52 (1988) 479.
[22] R.A. Cairns, A.A. Mamun, R. Bingham, R. Bostrom, R.O. Dendy, C.M.C. Nairn, P.K. Shukla, Geophys. Res. Lett. 22 (1995) 2709–2712.
[23] O.R. Rufai, R. Bharuthram, S.V. Singh, G.S. Lakhina, Phys. Plasmas 21 (2014) 082304.
[24] F.F. Chen, Introduction to Plasma Physics, 4th ed., Plenum Press, New York, 1974.
[25] M. Temerin, M. Woldorff, F.S. Mozer, Phys. Rev. Lett. 43 (1979) 1941–1943.
[26] A.A. Mamun, Phys. Rev. E 55 (1997) 1852.
[27] S.V. Singh, G.S. Lakhina, Nonlinear Process. Geophys. 11 (2) (2004) 275–279.
[28] C.R. Choi, K.W. Min, M.H. Woo, C.M. Ryu, Phys. Plasmas 17 (2010) 092904.
[29] O.R. Rufai, R. Bharuthram, S.V. Singh, G.S. Lakhina, Phys. Plasmas 23 (2016) 032309.